Progress In Electromagnetics Research, Vol. 124, 101–118, 2012

THE INTERFEROMETRY PHASE OF INSAR COHERENT JAMMING WITH ARBITRARY WAVEFORM MODULATION

Q. Liu*, S. Xing, X. Wang, J. Dong, D. Dai, and Y. Li

School of Electronic Science and Engineering, National University of Defense Technology, Changsha 410073, China

Abstract—This paper focuses on the interferometry phase of an active coherent jamming in InSAR (Interferometry Synthetic Aperture Radar) images. Based on the signal models of coherent jammer, the jamming's imaging results are derived by employing the Omega-K algorithm. By comparing the imaging results of InSAR's two channels, the jamming's interferometry phases for both working modes, the single-pass and repeat-pass modes, are proved to be constants. And the values of the interferometry phases are determined by the jammer's geometry position relative to InSAR baseline, but independent of the jamming's waveform modulation and its background terrain.

1. INTRODUCTION

The emerging of Synthetic Aperture Radar (SAR) in the 60's of last century is a milestone for two-dimensional radar imaging. Hitherto, there have still been many SAR technologies needed to be refined to achieve better system performances and image processing, e.g., two-dimensional sidelobe reduction [1], Automatic Target Recognition (ATR) [2, 3], sparse reconstruction with limited information available [4], etc. Also, its basic function of two-dimensional imaging has been extended to include many branches of SAR family, e.g., Polarimetric SAR (PolSAR) [5], multiband SAR [6], bistatic SAR [7, 8], Multi-Input Multi-Output SAR (MIMO SAR) [9], and Interferometry SAR (InSAR). Although InSAR has been developed since long time ago and widely used in many areas [10–12], its performance in a hostile electromagnetic environment has not

Received 16 November 2011, Accepted 6 January 2012, Scheduled 12 January 2012

* Corresponding author: Qingfu Liu (liu_675675@163.com).

yet been thoroughly studied. In real world, there exist many kinds of (intentional and/or not) jammings or interferences [13, 14], e.g., a civic TV transmitter, a radio station, or even a military jammer. Among all of the jammings, the military intentional jamming may prominently worsen the interferometry performance of InSAR. During the past two decades, many jamming-suppression methods have been developed to overcome the radio frequency interference (RFI) [15], and most of them are especially effective in the suppression of narrow band interference (NBI) [16]. RFI is usually produced unintentionally by the civil transmitters and can be suppressed in a relatively easier way. However, the jammings produced intentionally by a military jammer are usually much more difficult to be suppressed, since most of them share the same bandwidth with radar and their waveform modulations difficult to be known previously [17].

According to the coherence between jamming and SAR transmit signal, the jamming can be approximately divided into three types [17]. The first type is the incoherent jamming, which shares the same bandwidth but is incoherent to the SAR transmit signal in the fast time [18, 19]. The second type is known as the partially coherent jamming, which is coherent in the fast time but incoherent in the slow time [20, 21]. The third type is called the coherent jamming, which is coherent in both the fast and slow times [17, 22]. On the contrary, if the jamming can be detected by SAR, it can be canceled through a number of Electronic Counter-Counter Measures (ECCM) technologies, e.g., the wideband sidelobe-cancellation [23], the spatial filtering [24] and the adaptive beamforming [25].

The main purpose of this paper is to analyze the interferometry phase of a coherent jamming which is now widely employed in modern Digital Radio Frequency Memory (DRFM) based jammer. And the differences of the interferometry phases between the hostile jamming and the real targets may provide a new approach to distinguish them in the Electronic Counter Measures (ECM) environment. By the way, a SAR transponder [26–28] also works in a way very like the coherent jamming except that it is used for the calibration purpose and its signal parameters can be pre-known. In this point of view, both the coherent jammer and the transponder should have the same kind of interferometry phase if they are all with single transmit antenna. Thus, the results presented in the paper also hold true for an active transponder.

Table 1. The list of parameter names and their corresponding symbols.

Parameter Name	Symbol	Parameter Name	Symbol
The velocity of light	c	The Doppler frequency	f_a
The fast time	t_r	The carrier frequency of SAR transmitted signal	f_c
The slow time	t_a	The velocity of SAR platform	v_a
The minimum slant range between the slave antenna phase center and the transponder's transmit antenna phase center	R_s	The minimum slant range between the master antenna's phase center and the transponder's transmit antenna phase center	R_m
The fast time frequency	f_r	The reference slant range	R_{ref}

2. THE JAMMING'S INTERFEROMETRY PHASE IN REPEAT-PASS MODE

Firstly, we present the signal model of the jamming received by both master and slave channels of InSAR. The analytic expression of the jamming's two dimensional spectrum is derived by applying the principle of stationary phase (POSP) [29]. Then the Omega-K [29] algorithm is employed to derive the imaging result of the jamming. By comparing the imaging results of the master and the slave channels, the jamming's interferometry phase can be derived. The symbols that will be used in this paper are listed in Table 1.

2.1. The Jamming's Two-dimensional Spectrum

The "stop-and-go" approximation is widely used for SAR imaging with pulse transmit signal. For an ideal point-like target on the ground, its echo received by SAR is always delayed in accordance with the distance between the jammer and SAR system. And this will introduce the demodulated echo with a two-way delay in envelope and a quadratic modulation in phase. Interestingly, the jamming produced by a coherent jammer is similar to the point-like target's echo except that the baseband waveform can be arbitrarily modulated for the former. Therefore, the coherent jamming has a similar signal

model to that of point-like target's echo, if the jammer has only single transmit antenna. And its transmit signal received by InSAR master channel can be written as

$$g_m(t_r,t_a)=g\left(t_r-2R_m(t_a)c^{-1},t_a\right)\exp\left\{-j4\pi f_cR_m(t_a)c^{-1}\right\} \quad (1)$$

where $R_m(t_a)$ is the slant range between the antenna phase centers of InSAR master channel and the transponder with respect to different slow time t_a, namely,

$$R_m(t_a)=\sqrt{R_m^2+v_a^2t_a^2} \quad (2)$$

$g(t_r,t_a)$ represents the base band component or the arbitrary waveform modulation of the transponder's transmitted signal. The second term in (1) is caused by the carrier frequency modulation. If the Fourier transform of $g(t_r,t_a)$ with respect to t_r is denoted as

$$G(f_r,t_a)\triangleq fT\{g(t_r,t_a)\} \quad (3)$$

Then the Fourier transform of $g\left[t_r-2c^{-1}R_m(t_a),t_a\right]$ can be expressed as

$$fT\left\{g\left[t_r-2c^{-1}R_m(t_a),t_a\right]\right\}=\exp\left\{-j4\pi f_rc^{-1}R_m(t_a)\right\}G(f_r,t_a) \quad (4)$$

And the Fourier transform of $g_m(t_r,t_a)$ in (1) can be written as

$$\begin{aligned}G_m(f_r,t_a)&=fT\left\{g\left(t_r-2R_m(t_a)c^{-1},t_a\right)\exp\left\{-j4\pi f_cR_m(t_a)c^{-1}\right\}\right\}\\&=G(f_r,t_a)\exp\left\{j\theta_{m-1}(f_r,t_a)\right\}\end{aligned} \quad (5)$$

where

$$\theta_{m-1}(f_r,t_a)=-4\pi(f_c+f_r)R_m(t_a)c^{-1} \quad (6)$$

There are two terms in (5), the first one is a slow-changing part with respect to t_a, and the second is a fast-changing part. Also, the Fourier transform of $G_m(f_r,t_a)$ in (5) with respect to t_a can be obtained by applying the POSP directly to (5) as follows

$$\begin{aligned}G_m(f_r,f_a)&=\int G(f_r,t_a)\exp\left\{-j4\pi(f_c+f_r)R_m(t_a)c^{-1}\right\}\exp\left\{-j2\pi f_at_a\right\}dt_a\\&=\int G(f_r,t_a)\exp\left\{j\theta_{m-2}(f_r,t_a)\right\}dt_a\end{aligned} \quad (7)$$

where

$$\begin{aligned}\theta_{m-2}(f_r,t_a)&=2\pi\left[-f_at_a-2(f_c+f_r)R_m(t_a)c^{-1}\right]\\&=2\pi\left[-f_at_a-2(f_c+f_r)c^{-1}\sqrt{R_m^2+v_a^2t_a^2}\right]\end{aligned} \quad (8)$$

The partial derivative of $\theta_{m-2}(f_r,t_a)$ with respect to t_a can be expressed as

$$\frac{\partial\theta_{m-2}(f_r,t_a)}{\partial t_a}=2\pi\left[-f_a-\frac{2(f_c+f_r)v_a^2t_a}{c\sqrt{R_m^2+v_a^2t_a^2}}\right] \quad (9)$$

Then the stationary point of the integrand in (7) can be derived as

$$t_a = -\frac{cf_aR_m}{v_a\sqrt{\left[2\left(f_c+f_r\right)v_a\right]^2-\left(cf_a\right)^2}} \tag{10}$$

By substituting (10) into (7), the integral result can be gotten as

$$G_m\left(f_r,f_a\right) = G_1\left(f_r,f_a\right)\exp\left\{j\theta_{m-3}\left(f_r,f_a\right)\right\} \tag{11}$$

where

$$G_1\left(f_r,f_a\right) = G\left(f_r,-\frac{cf_aR_m}{v_a\sqrt{\left[2\left(f_c+f_r\right)v_a\right]^2-\left(cf_a\right)^2}}\right) \tag{12}$$

and

$$\begin{aligned}\theta_{m-3}\left(f_r,f_a\right) &= \theta_{m-2}\left(f_r,-\frac{cf_aR_m}{v_a\sqrt{\left[2\left(f_c+f_r\right)v_a\right]^2-\left(cf_a\right)^2}}\right)\\ &= -\frac{4\pi R_m}{c}\sqrt{\left(f_c+f_r\right)^2-\frac{c^2f_a^2}{4v_a^2}}\end{aligned} \tag{13}$$

Now the jamming received by the master channel has been expressed in two-dimensional frequency domain. Obviously, this expression does not depend on the SAR imaging algorithm itself, but depend on the parameters of the SAR transmit signals, the modulation of the jammer, and the relative geometric positions between SAR and the jammer, etc..

2.2. The Jamming's Imaging Results and Its Interferometry Phase

In this part of the paper, it is the imaging result of the jamming that makes the main concern. Without loss generality, the Omega-K algorithm is used in the following imaging process, where the reference phase term in the Omega-K algorithm can be written as [29]

$$\theta_{ref}\left(f_r,f_a\right) = -\frac{\pi f_r^2}{K_r}+\frac{4\pi R_{ref}}{c}\sqrt{\left(f_c+f_r\right)^2-\frac{c^2f_a^2}{4V_a^2}} \tag{14}$$

Multiply (11) with the reference phase term in (14) to generate

$$\begin{aligned}&G_m\left(f_r,f_a\right)\cdot\exp\left\{j\theta_{ref}\left(f_r,f_a\right)\right\}\\ =&\left\{\exp\left\{-j\frac{4\pi R_m}{c}\sqrt{\left(f_c+f_r\right)^2-\frac{c^2f_a^2}{4v_a^2}}\right\}\cdot G_1\left(f_r,f_a\right)\right\}\\ &\cdot\exp\left\{j\theta_{ref}\left(f_r,f_a\right)\right\}\triangleq G'_m\left(f_r,f_a\right)\end{aligned} \tag{15}$$

By applying the Stolt mapping [29]

$$\sqrt{(f_c+f_r)^2-\frac{c^2f_a^2}{4v_a^2}}=f_c+f_r' \tag{16}$$

(15) can be transformed to

$$\begin{aligned}G_m'\left(f_r',f_a\right)=&G_1\left(\sqrt{\left(f_c+f_r'\right)^2+\frac{c^2f_a^2}{4v_a^2}}-f_c,f_a\right)\\&\exp\left\{-j\frac{\pi}{K_r}\left[\sqrt{\left(f_c+f_r'\right)^2+\frac{c^2f_a^2}{4v_a^2}}-f_c\right]^2\right\}\\&\times\exp\left\{-j4\pi\left(R_m-R_{ref}\right)c^{-1}\left(f_c+f_r'\right)\right\}\\&\triangleq G_2\left(f_r',f_a\right)\cdot\exp\left\{-j4\pi\left(R_m-R_{ref}\right)c^{-1}\left(f_c+f_r'\right)\right\}\end{aligned}\tag{17}$$

where

$$\begin{aligned}G_2\left(f_r',f_a\right)=&\ G_1\left(\sqrt{\left(f_c+f_r'\right)^2+\frac{c^2f_a^2}{4v_a^2}}-f_c,f_a\right)\\&\exp\left\{-j\frac{\pi}{K_r}\left[\sqrt{\left(f_c+f_r'\right)^2+\frac{c^2f_a^2}{4v_a^2}}-f_c\right]^2\right\}\end{aligned}\tag{18}$$

The jamming's imaging result by using the Omega-K algorithm can be obtained through the two-dimensional inverse Fourier transform of (17)

$$g_m(t_r,t_a)=g_2\left(t_r-2\left(R_m-R_{ref}\right)c^{-1},t_a\right)\exp\left\{-j4\pi\left(R_m-R_{ref}\right)c^{-1}f_c\right\} \tag{19}$$

where $g_2\left(t_r,t_a\right)$ is the two dimensional inverse Fourier transform of $G_2\left(f_r',f_a\right)$. Being similar to (1), the jamming received by the slave channel is

$$g_s\left(t_r,t_a\right)=g\left(t_r-2R_m\left(t_a\right)c^{-1},t_a\right)\exp\left\{-j4\pi f_cR\left(t_a\right)c^{-1}\right\} \tag{20}$$

After the imaging process, the imaging output of the slave channel is

$$g_s\left(t_r,t_a\right)=g_2\left(t_r-2\left(R_s-R_{ref}\right)c^{-1},t_a\right)\exp\left\{-j4\pi\left(R_s-R_{ref}\right)c^{-1}f_c\right\} \tag{21}$$

The difference between $t_r-2c^{-1}(R_m-R_{ref})$ and $t_r-2c^{-1}\left(R_s-R_{ref}\right)$ in both (20) and (21) will induce a envelope shift between $g_m\left(t_r,t_a\right)$ and $g_s\left(t_r,t_a\right)$ (i.e., the 2-D imaging results of the two channels of InSAR). This effect can be compensated by the image

registration processing of InSAR. Here we suppose that the slave image is adjusted in accordance with the master image, then $g_s(t_r, t_a)$ should be rearranged as

$$g_s(t_r, t_a) = g_2\left(t_r - 2(R_m - R_{ref})c^{-1}, t_a\right)\exp\left\{-j4\pi(R_s - R_{ref})c^{-1}f_c\right\} \quad (22)$$

By comparing the second terms in both (19) and (22), the interferometry phase of jamming can be obtained as

$$\theta_{IF} = 4\pi(R_m - R_s)c^{-1}f_c \quad (23)$$

Note that the interferometry phase given in (23) is a constant, which is irrelevant to the fast time t_r and slow time t_a, and independent of the jamming's waveform modulations. Indeed, it is equal to the interferometry phase of the terrain where the jammer lies in. In other words, the interferometry phase of the jamming is determined by the jammer's geometry position relative to InSAR's two channels.

3. THE JAMMING'S INTERFEROMETRY PHASE IN SINGLE-PASS MODE

In single-pass mode, the jamming received by the master channel is the same as the one in repeat-pass mode which is given in (1). Therefore, its imaging result is also the same as that expressed in (19), and will not be discussed anymore in the following part. However, the jamming received by the slave channels are different from each other for both repeat-pass and single-pass modes, where the latter can be expressed as

$$\begin{aligned} g_s(t_r, t_a) &= g\left(t_r - [R_m(t_a) + R_s(t_a)]c^{-1}, t_a\right) \\ &\quad \exp\left\{-j2\pi f_c c^{-1}[R_m(t_a) + R_s(t_a)]\right\} \end{aligned} \quad (24)$$

Compared with (1), it should be noted that the two-way time delay in (1) is now replaced with the summation of two separate delays. In order to apply the Omega-K algorithm to (24), the jamming's two dimensional spectrum should be derived as follows. According to the expression of (4), the Fourier transform of $g_s(t_r, t_a)$ with respect to t_r can be written as

$$G_s(f_r, t_a) = G(f_r, t_a)\exp\left\{-j2\pi(f_c + f_r)c^{-1}[R_m(t_a) + R_s(t_a)]\right\} \quad (25)$$

where the first and second terms are both the slow changing and fast changing parts with respect to the slow time t_a. Therefore, the POSP can also be applied to (25) to derive the two-dimensional spectrum.

The Fourier transform of the second term in (25) can be expressed as

$$\begin{aligned} & fT\left(\exp\left\{-j2\pi\left(f_c+f_r\right)\left[R_m\left(t_a\right)+R_s\left(t_a\right)\right]c^{-1}\right\}\right) \\ = & \int \exp\left\{-j2\pi\left(f_c+f_r\right)\left[R_m\left(t_a\right)+R_s\left(t_a\right)\right]c^{-1}\right\}\exp\{-j2\pi f_a t_a\}\,dt_a \\ \triangleq & \int \exp\left\{-j\theta\left(f_r,t_a\right)\right\}dt_a \end{aligned} \tag{26}$$

where

$$\begin{aligned} \theta\left(f_r,t_a\right) = & 2\pi\left[-f_a t_a-\left(f_c+f_r\right)\left[R_m\left(t_a\right)+R_s\left(t_a\right)\right]c^{-1}\right] \\ = & 2\pi\left[-f_a t_a-c^{-1}\left(f_c+f_r\right)\left(\sqrt{R_m^2+v_a^2t_a^2}+\sqrt{R_s^2+v_a^2t_a^2}\right)\right] \end{aligned} \tag{27}$$

It is a difficult task to resolve the integral in (26). Therefore, an approximation is made in the following to resolve this problem. If the difference between the two slant ranges R_m and R_s is expressed as

$$\delta_R = R_m - R_s \tag{28}$$

Then the first square root in (27) can be approximated as

$$\begin{aligned} \sqrt{R_m^2+v_a^2t_a^2} &= \sqrt{\left(R_s+\delta_R\right)^2+v_a^2t_a^2} \\ &= \sqrt{R_s^2+2R_s\delta_R+\delta_R^2+v_a^2t_a^2} \end{aligned} \tag{29}$$

Considering $\delta_R \ll R_s$ and $\delta_R \ll v_a t_a$, it has $\delta_R^2 \ll R_s^2$ and $\delta_R^2 \ll v_a^2 t_a^2$. So (29) can be approximated as

$$\sqrt{R_m^2+v_a^2t_a^2} \approx \sqrt{R_s^2+2R_s\delta_R+v_a^2t_a^2} \tag{30}$$

It is useful to make the following parabolic approximation

$$\sqrt{R_m^2+v_a^2t_a^2} \approx \sqrt{R_s^2+v_a^2t_a^2}+\frac{R_s}{\sqrt{R_s^2+v_a^2t_a^2}}\delta_R \tag{31}$$

The parabolic approximation can also be applied to the square root term $\sqrt{R_m^2+v_a^2t_a^2}$ in (27) to yield

$$\begin{aligned} \theta(f_r,t_a) \approx & 2\pi\left[-f_a t_a-\frac{f_c+f_r}{c}\left(\sqrt{R_s^2+v_a^2t_a^2}+\frac{R_s}{\sqrt{R_s^2+v_a^2t_a^2}}\delta_R+\sqrt{R_s^2+v_a^2t_a^2}\right)\right] \\ = & 2\pi\left[-f_a t_a-\frac{f_c+f_r}{c}\left(2\sqrt{R_s^2+v_a^2t_a^2}+\frac{R_s}{\sqrt{R_s^2+v_a^2t_a^2}}\delta_R\right)\right] \end{aligned} \tag{32}$$

Then the first derivative of $\theta\left(f_r,t_a\right)$ with respect to t_a can be written as

$$\theta'\left(f_r,t_a\right) = 2\pi\left[-f_a-\frac{\left(f_c+f_r\right)}{c}\left(\frac{2v_a^2t_a}{\sqrt{R_s^2+v_a^2t_a^2}}-\frac{R_s v_a^2 t_a}{\left(R_s^2+v_a^2t_a^2\right)^{3/2}}\delta_R\right)\right] \tag{33}$$

It has the following inequality

$$\frac{R_s v_a^2 t_a}{(R_s^2+v_a^2t_a^2)^{3/2}}\left|\delta_R\right| \le \frac{v_a^2 t_a}{R_s^2+v_a^2t_a^2}\left|\delta_R\right| = \frac{2v_a^2t_a}{\sqrt{R_s^2+v_a^2t_a^2}}\frac{\left|\delta_R\right|}{2\sqrt{R_s^2+v_a^2t_a^2}} \quad (34)$$

For $\frac{|\delta_R|}{2\sqrt{R_s^2+v_a^2t_a^2}} \ll 1$, then

$$\frac{2v_a^2t_a}{\sqrt{R_s^2+v_a^2t_a^2}}\frac{\left|\delta_R\right|}{2\sqrt{R_s^2+v_a^2t_a^2}} \ll \frac{2v_a^2t_a}{\sqrt{R_s^2+v_a^2t_a^2}} \quad (35)$$

Namely,

$$\frac{R_s v_a^2 t_a}{(R_s^2+v_a^2t_a^2)^{3/2}}\left|\delta_R\right| \ll \frac{2v_a^2t_a}{\sqrt{R_s^2+v_a^2t_a^2}} \quad (36)$$

According to the inequality given by (36), the second term in the bracket of (33) can be neglected, and $\theta'(f_r,t_a)$ can be approximated as

$$\theta'(f_r,t_a) \approx 2\pi\left[-f_a - \frac{f_c+f_r}{c}\frac{2v_a^2t_a}{\sqrt{R_s^2+v_a^2t_a^2}}\right] \quad (37)$$

By setting the value of $\theta'(f_r,t_a)$ equal to zero, the stationary point of the integrand in (26) can be written as

$$t_a = -\frac{cf_aR_s}{2v_a^2\sqrt{(f_c+f_r)^2-\frac{c^2f_a^2}{4v_a^2}}} \quad (38)$$

By substituting (31) and (38) into (27), the stationary point of the phase can be expressed as (shown in the appendix)

$$\begin{aligned}\theta&\left(f_r,-\frac{cf_aR_s}{2v_a^2\sqrt{(f_c+f_r)^2-\frac{c^2f_a^2}{4v_a^2}}}\right)\\ &\approx -\frac{4\pi R_s}{c}\sqrt{(f_c+f_r)^2-\frac{c^2f_a^2}{4v_a^2}} - \frac{2\pi}{c}\sqrt{(f_c+f_r)^2-\frac{c^2f_a^2}{4v_a^2}}\delta_R \quad (39)\end{aligned}$$

By applying POSP to (25), its Fourier transform of $G_s(f_r,t_a)$ with respect to t_a can be written as

$$\begin{aligned}G_s(f_r,f_a) &= \exp\left\{j\left[-\frac{4\pi R_s}{c}\sqrt{(f_c+f_r)^2-\frac{c^2f_a^2}{4v_a^2}}\right.\right.\\ &\quad\left.\left.-\frac{2\pi}{c}\sqrt{(f_c+f_r)^2-\frac{c^2f_a^2}{4v_a^2}}\delta_R\right]\right\}G_1(f_r,f_a) \quad (40)\end{aligned}$$

Now we have derived the jamming's two-dimensional spectrum $G_s(f_r, f_a)$, which is needed for the Omega-K algorithm. Multiplying (40) with the reference function shown in (14), it has

$$\begin{aligned} & G_s(f_r, f_a) \cdot \exp\{j\theta_{ref}(f_r, f_a)\} \\ = \; & G_1(f_r, f_a) \cdot \exp\{j\theta_{ref-1}(f_r, f_a)\} \triangleq G'_s(f_r, f_a) \end{aligned} \tag{41}$$

where

$$\begin{aligned} \theta_{ref-1}(f_r, f_a) \; = \; & -\frac{4\pi(R_s - R_{ref})}{c}\sqrt{(f_c + f_r)^2 - \frac{c^2 f_a^2}{4v_a^2}} \\ & -\frac{2\pi\delta_R}{c}\sqrt{(f_c + f_r)^2 - \frac{c^2 f_a^2}{4v_a^2}} - \frac{\pi f_r^2}{K_r} \end{aligned} \tag{42}$$

By applying the Stolt mapping presented in (16), (41) can be transformed to

$$\begin{aligned} G'_s(f'_r, f_a) = & G_1\left(\sqrt{(f_c + f'_r)^2 + \frac{c^2 f_a^2}{4v_a^2}} - f_c, f_a\right) \\ & \cdot \exp\left\{-j\frac{\pi}{K_r}\left[\sqrt{(f_c + f'_r)^2 + \frac{c^2 f_a^2}{4v_a^2}} - f_c\right]^2\right\} \\ & \times \exp\left\{-j\frac{4\pi(R_s - R_{ref} + 0.5\delta_R)}{c}(f_c + f'_r)\right\} \\ = & G_2(f'_r, f_a) \cdot \exp\left\{-j\frac{4\pi(R_s - R_{ref} + 0.5\delta_R)}{c}(f_c + f'_r)\right\} \end{aligned} \tag{43}$$

Then the two-dimensional inverse Fourier transform of (41) can be expressed as

$$\begin{aligned} g_s(t_r, t_a) \; = \; & g_2\left(t_r - 2c^{-1}(R_s - R_{ref} + 0.5\delta_R), t_a\right) \\ & \exp\left\{-j4\pi(R_s - R_{ref} + 0.5\delta_R)c^{-1}f_c\right\} \end{aligned} \tag{44}$$

After image registration processing of InSAR, the slave image $g_m(t_r, t_a)$ should be rewritten as

$$\begin{aligned} g_m(t_r, t_a) \; = \; & g_2\left(t_r - 2(R_s - R_{ref})c^{-1}, t_a\right) \\ & \exp\left\{-j4\pi(R_s - R_{ref} + 0.5\delta_R)c^{-1}f_c\right\} \end{aligned} \tag{45}$$

As mentioned above, the imaging results of the master channel can also be expressed as (19). Then the interferometry phase of

the jamming in the single pass mode can be derived by comparing the imaging results of the master and slave channels, i.e., the phase difference between (19) and (45). And it can be written as

$$\theta_{IF} = 2\pi\delta_R c^{-1} f_c = 2\pi \left(R_m - R_s\right) c^{-1} f_c \tag{46}$$

By comparing (23) and (46), it can be seen that the values of the jamming's interferometry phase for both repeat-pass and single-pass modes are constants. Both of them have the same interferometry value which is determined by the geometric position of the jammer, and is independent of the jammer's waveform modulations.

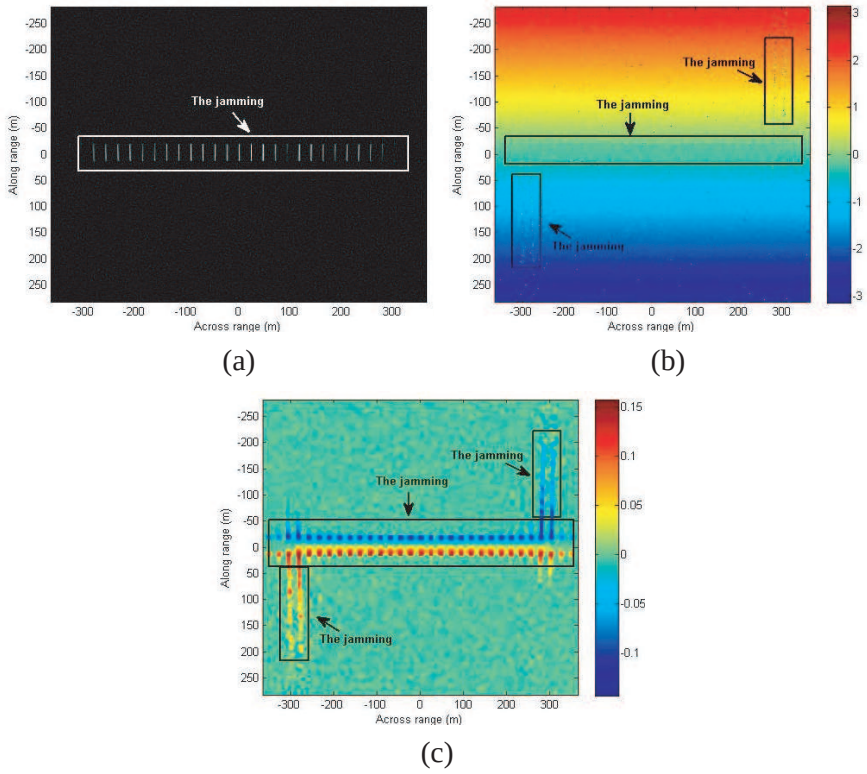

Figure 1. The InSAR images of the jamming with periodic modulation. (a) The 2-D image of the master channel. (b) The interferometry phase. (c) The interferometry phase after removing the flat earth phase and phase filtering.

4. SIMULATION AND ANALYSIS

To further analyze the interferometry phase of the jamming, a simulation of airborne InSAR is presented in this part. Since the simulation of SAR echoes with large scene is rather computational expensive [30], the images with complex Gaussian clutter are employed here without resorting to echoes simulation. The InSAR parameters are listed as follows. The baseline length is 2 m, the flight height is 8 km, the baseline depression angle is 60 deg. Both the first and the second simulation scenarios share the same terrain, which is a flat plane with an area of 500 m × 500 m in both the ground range and vertical directions. The jammer is in the center of the terrain. The jamming-to-clutter power ratio (JCR) is 6 dB. The 2-D images for both the master and slave channels are similar to each other in magnitude, so only the master image is presented (as shown in Figure 1(a)).

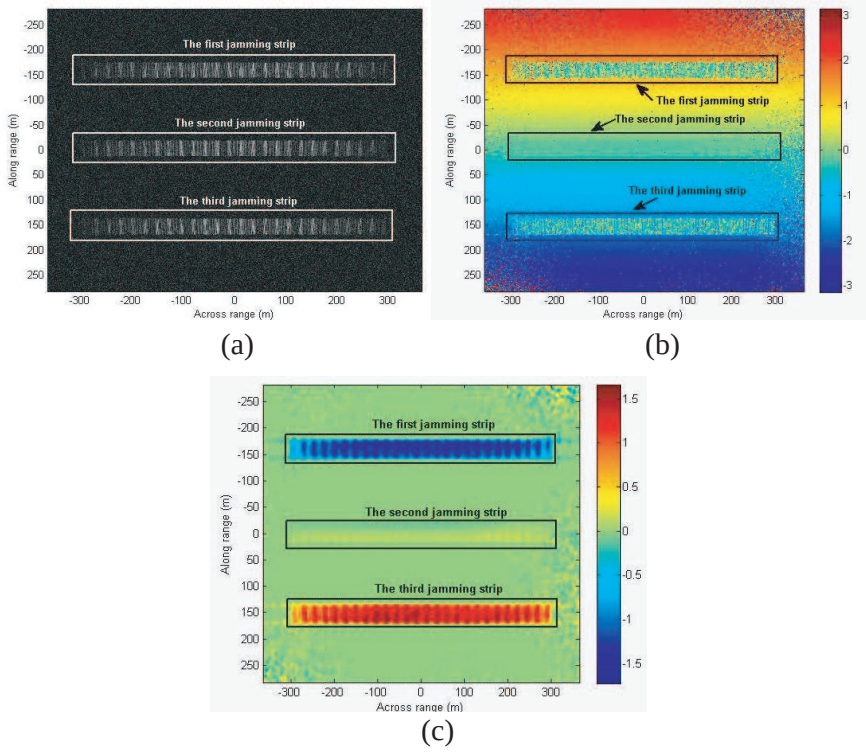

Figure 2. The InSAR images of the jamming with periodic and multi-delay modulations. (a) The 2-D imaging result of the master channel. (b) The interferometry phase. (c) The interferometry phase after removing the flat earth phase and phase filtering.

The periodic modulation jamming [17] is utilized in the first simulation scenario, and this kind of jamming can produce multiple discrete lines in the across range direction (as shown in Figure 1(a)). The interferometry phase of the jamming does not show much difference from that of the terrain, because the jamming is distributed around the jammer and because the flat ground phase does not change drastically within a limited ground range (shown in Figure 1(b)). After the removal of the flat ground phase, the interferometry phase of the terrain become null, whereas a phase opposite to the flat ground phase is added to the jamming (as shown in Figure 1(c)). Therefore, the value of the jamming's interferometry phase should be a constant in the original InSAR interferometry image given in Figure 1(b).

The multi-delay modulation is employed along with the periodic modulation by the jammer in the second simulation scenario. This kind of modulation can produce multi jamming strip along the ground range direction (as shown in Figure 2(a)). There are three jamming strips in Figure 2(a), where the first and the third strips are before and after the jammer in the ground range direction, respectively; the second strip is around the jammer. As shown in Figure 2(b), all of the

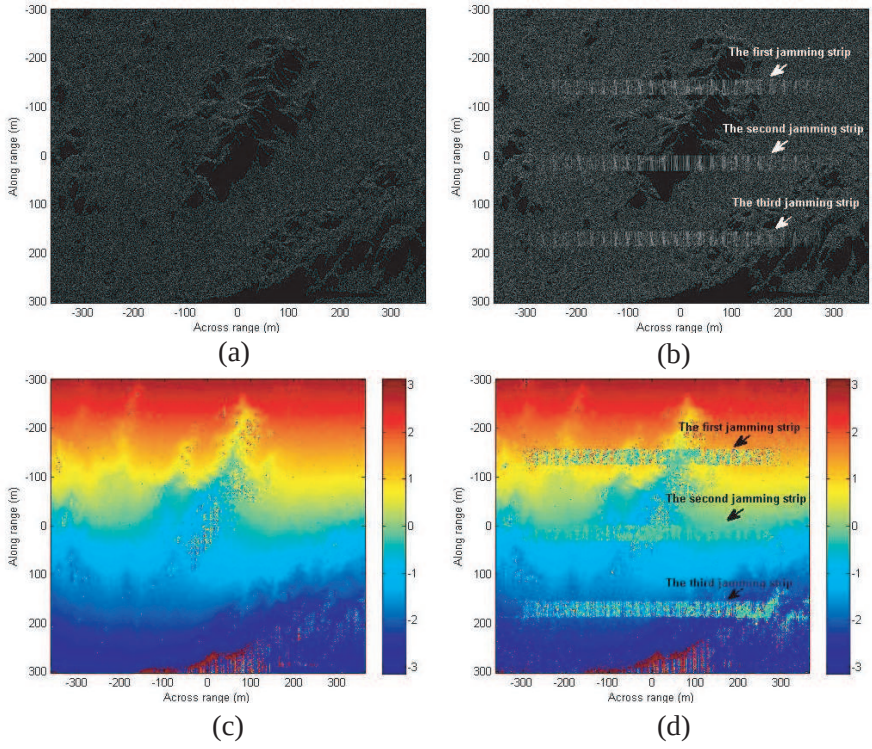

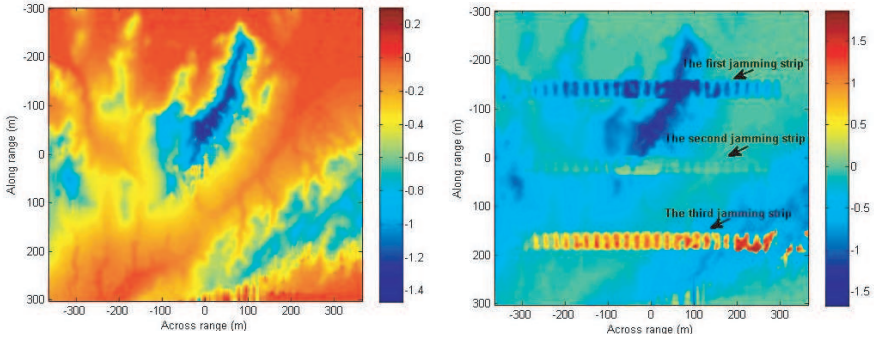

(e) (f)

Figure 3. The InSAR images of the jamming with periodic and multi-delay modulations. (a) The 2-D imaging result of the master channel (jamming-free). (b) The 2-D imaging result of the master channel (being jammed). (c) The interferometry phase (jamming-free). (d) The interferometry phase (being jammed). (e) The interferometry phase after removing the flat earth phase and phase filtering (jamming-free). (f) The interferometry phase after removing the flat earth phase and phase filtering (being jammed).

three jammings share the same interferometry phase, and are equal to the interferometry phase of the terrain where the jammer lies in. The first and the third jamming strips can be easily distinguished from the background interferometry phase, since they are away from the jammer in the ground range direction. After the removal of the flat ground phase, all of the three jamming strips are added with an opposite flat ground phase (as shown in Figure 2(c)).

A terrain with height variation is used in the third simulation scenario. Some dark areas can be seen in Figures 3(a) and (b). They are indeed the shadows of the mountains. The same jamming is used in both the second and third simulation scenarios. As shown in Figure 3, the jamming in the third simulation scenario have the same interferometry phase as that in the second one. Therefore, the interferometry phase of the jamming in the InSAR images are independent from its background terrain.

5. CONCLUSION

For both the repeat-pass and single-pass modes, the interferometry phases of the jamming are constants. They are equal to the interferometry phases of terrain where the jammer lies in and independent of the jamming's waveform modulations. Although only

the case of the coherent jammer is discussed throughout this paper, the interferometry phase of any other coherent active transmitter with single transmit antenna should be a constant. This will also hold true for a SAR transponder when it is used for calibration purpose. Therefore, the work of this paper can be developed to recognize the active coherent transmitter in InSAR images.

APPENDIX A. THE JAMMING'S STATIONARY POINT PHASE IN INSAR SLAVE CHANNEL

Substituting (31) into (27) yields:

$$\theta\left(f_r,t_a\right)\approx 2\pi\left[-f_a t_a - c^{-1}\left(f_c+f_r\right)\left(2\sqrt{R_s^2+v_a^2t_a^2}+\frac{R_s}{\sqrt{R_s^2+v_a^2t_a^2}}\delta_R\right)\right] \quad \text{(A1)}$$

Substituting (38) into $\sqrt{R_s^2+v_a^2t_a^2}$ yields:

$$\sqrt{R_s^2+v_a^2t_a^2}\Big|_{t_a=-\frac{cf_aR_s}{2v_a^2\sqrt{(f_c+f_r)^2-\frac{c^2f_a^2}{4v_a^2}}}} = \sqrt{R_s^2+\frac{\left(cf_aR_s\right)^2}{4v_a^2\left[\left(f_c+f_r\right)^2-\frac{c^2f_a^2}{4v_a^2}\right]}}$$

$$=\sqrt{\frac{4v_a^2\left(f_c+f_r\right)^2R_s^2}{4v_a^2\left[\left(f_c+f_r\right)^2-\frac{c^2f_a^2}{4v_a^2}\right]}}=\frac{\left(f_c+f_r\right)R_s}{\sqrt{\left(f_c+f_r\right)^2-\frac{c^2f_a^2}{4v_a^2}}} \quad \text{(A2)}$$

Therefore, (39) can be derived as

$$\begin{aligned}
&\theta\left(f_r,-\frac{cf_aR_s}{2v_2^2\sqrt{(f_c+f_r)^2-\frac{c^2f_a^2}{4v_a^2}}}\right)\\
&\approx 2\pi\left[\frac{cf_aR_s}{2v_2^2\sqrt{(f_c+f_r)^2-\frac{c^2f_a^2}{4v_a^2}}}\right.\\
&\quad\left.-\frac{f_c+f_r}{c}\left(\frac{2f_c+f_rR_s}{\sqrt{(f_c+f_r)^2-\frac{c^2f_a^2}{4v_a^2}}}+\frac{\sqrt{(f_c+f_r)^2-\frac{c^2f_a^2}{4v_a^2}}}{f_c+f_r}\delta_R\right)\right]\\
&=2\pi\left[\frac{c^2f_aR_s-4v_a^2(f_c+f_r)^2R_s}{2v_2^2\sqrt{(f_c+f_r)^2-\frac{c^2f_a^2}{4v_a^2}}}-c^{-1}\sqrt{(f_c+f_r)^2-\frac{c^2f_a^2}{4v_a^2}}\delta_R\right]\\
&=-\frac{4\pi R_s}{c}\sqrt{(f_c+f_r)^2-\frac{c^2f_a^2}{4v_a^2}}-\frac{2\pi}{c}\sqrt{(f_c+f_r)^2-\frac{c^2f_a^2}{4v_a^2}}\delta_R \quad \text{(A3)}
\end{aligned}$$

REFERENCES

1. Woo, J.-C., B.-G. Lim, and Y.-S. Kim, "Modification of the recursive sidelobe minimization technique for the range-doppler algorithm of SAR imaging," *Journal of Electromagnetic Waves and Applications*, Vol. 25, No. 13, 1783–1794, 2011.
2. Park, S.-H., M.-G. Joo, and K.-T. Kim, "Construction of ISAR training database for automatic target recognition," *Journal of Electromagnetic Waves and Applications*, Vol. 25, No. 11–12, 1493–1503, 2011.
3. Han, S.-K, H.-T. Kim, S.-H. Park, and K.-T. Kim, "Efficient radar target recognition using a combination of range profile and time-frequency analysis," *Progress In Electromagnetics Research*, Vol. 108, 131–140, 2010.
4. Wei, S.-J., X.-L. Zhang, J. Shi, and G. Xiang, "Sparse reconstruction for SAR imaging based on compressed sensing," *Progress In Electromagnetics Research*, Vol. 109, 63–81, 2010.
5. Jin, Y.-Q., "Polarimetric scattering modeling and information retrieval of SAR remote sensing — A review of fdu work," *Progress In Electromagnetics Research*, Vol. 104, 333–384, 2010.
6. Teng, H. T., H.-T. Ewe, and S. L. Tan, "Multifractal dimension and its geometrical terrain properties for classification of multi-band multi-polarized SAR image," *Progress In Electromagnetics Research*, Vol. 104, 221–237, 2010.
7. Dai, C. and X.-L. Zhang, "Omega-K algorithm for bistatic SAR with arbitrary geometry configuration," *Journal of Electromagnetic Waves and Applications*, Vol. 25, No. 11–12, 1564–1576, 2011.
8. Sun, J., S. Mao, G. Wang, and W. Hong, "Polar format algorithm for spotlight bistatic SAR with arbitrary geometry configuration," *Progress In Electromagnetics Research*, Vol. 103, 323–338, 2010.
9. Lim, S.-H., C. G. Hwang, S.-Y. Kim, and N.-H. Myung, "Shifting MIMO SAR system for high-resolution wide-swath imaging," *Journal of Electromagnetic Waves and Applications*, Vol. 25, No. 8–9, 1168–1178, 2011.
10. Schneider, R. Z., K. P. Papathanassiou, I. Hajnsek, and A. Moreira, "Polarimetric and interferometric characterization of coherent scatterers in urban areas," *IEEE Trans. Geosci. Remote Sens.*, Vol. 44, No. 4, 971–984, Apr. 2006.
11. Krieger, G., I. Hajnsek, K. P. Papathanassiou, M. Younis, et al., "Interferometric synthetic aperture radar (SAR) missions employing formation flying," *Proceeding of IEEE*, Vol. 98, No. 5,

816–843, May 2010.

12. Felguera-Martín, D., J.-T. González-Partida, P. Almorox-González, M. Burgos-García, and B.-P. Dorta-Naranjo, "Interferometric inverse synthetic aperture radar experiment using an interferometric linear frequency modulated continuous wave millimeter-wave radar," *IET Radar Sonar Navig.*, Vol. 5, No. 1, 39–47, 2011.
13. Vu, V. T., T. K. Sjogren, M. I. Pettersson, L. Håkansson, A. Gustavsson, and L. M. H. Ulander, "RFI suppression in ultrawideband SAR using an adaptive line enhancer," *IEEE Geoscience and Remote Sensing Letters*, Vol. 7, No. 4, 694–698, Oct. 2010.
14. Reigber, A. and L. Ferro-Famil, "Interference suppression in synthesized SAR images," *IEEE Geoscience and Remote Sensing Letters*, Vol. 2, No. 1, 45–49, Jan. 2005.
15. Lord, R. T. and M. R. Inggs, "Efficient RFI suppression in SAR using LMS adaptive filter integrated with range/Doppler algorithm," *Electronics Letters*, Vol. 35, No. 8, 629–630, Apr. 1999.
16. Miller, T., L. Potter, and J. McCorkle, "RFI suppression for ultra wideband radar," *IEEE Trans. on Aerospace and Electronic Systems*, Vol. 33, No. 4, 1142–1156, Oct. 1997.
17. Liu, Q., S. Xing, X. Wang, J. Dong, and D. Dai, "A stripmap SAR coherent jammer structure utilizing periodic modulation technology," *Progress In Electromagnetics Research B*, Vol. 28, 111–128, 2011.
18. Condley, C. J., "Some system considerations for electronic countermeasures to synthetic aperture radar," *IEE Colloquium on Electronic Warfare Systems*, London, 1991.
19. Dumper, K., P. S. Cooper, A. N. F. Wons, C. J. Condley, and P. Tully, "Spaceborne synthetic aperture radar and noise jamming," *Proc. IEE Radar*, 411–414, 1997.
20. Wu, X., D. Dai, and X. Wang, "Study on SAR jamming measures," *IET International Conference on Radar Systems,* 176–179, Edinburgh, England, 2007.
21. Wu, X., D. Dai, X. Wang, and H. Lu, "Evaluation of SAR jamming performance, " *MAPE 2007*, 1476–1479, Hangzhou, 2007.
22. Dai, D., X. Wu, X. Wang, and S.-P. Xiao, "SAR active-decoys jamming based on DRFM," *IET International Conference on Radar Systems*, 2007.

23. Mrstik, V., "Agile-beam synthetic aperture radar opportunities," *IEEE Trans. on AES*, Vol. 34, No. 2, 500–507, Apr. 1998.
24. Ender, J. H. G., P. Berens, A. R. Brenner, L. Roing, and U. Skupin, "Multi channel SAR/MTI system development at FGAN: From AER to PAMIR," *2002 IEEE International Geoscience and Remote Sensing Symposium,* Vol. 3, 1697–1701, 2002.
25. Paine, A. S., "An adaptive beamforming technique for countering synthetic aperture radar (SAR) jamming threats," *2007 IEEE Radar Conf.*, 630–634, Apr. 2007
26. Kemp, W. M. and N. M. Martin, "A synthetic aperture radar calibration transponder at C-band," *Record of the IEEE 1990 International Radar Conference*, 81–85, May 1990.
27. Weiss, M. and P. Berens, "Motion compensation of wideband synthetic aperture radar with a new transponder technique," *2002 Geoscience and Remote Sensing Symposium*, Vol. 6, 3649–3651, Jun. 2002.
28. Mohr, J. J. and S. N. Madsen,"Geometric calibration of ERS satellite SAR images," *IEEE Trans. on Geoscience and Remote Sensing*, Vol. 39, No. 4, 842–850, Apr. 2001.
29. Cumming, I. G., and F. H. Wong, *Digital Processing of Synthetic Aperture Radar Data,* 2004.
30. Zhao, Y. W., M. Zhang, and H. Chen, "An efficient ocean SAR raw signal simulation by employing fast fourier transform," *Journal of Electromagnetic Waves and Applications*, Vol. 24, No. 16, 2273–2284, 2010.